JOURNAL OF GEOPHYSICAL RESEARCH, VOL. 113, D16S37, doi:10.1029/2007JD008858, 2008

Implementation of cloud retrievals for TES atmospheric retrievals: 2. Characterization of cloud top pressure and effective optical depth retrievals

Annmarie Eldering,[1] Susan S. Kulawik,[1] John Worden,[1] Kevin Bowman,[1] and Greg Osterman[1]

Received 19 April 2007; revised 11 February 2008; accepted 20 March 2008; published 10 June 2008.

[1] We characterize and validate the cloud products from the Tropospheric Emission Spectrometer (TES) by comparing TES estimates of effective cloud optical depth and cloud top height to those from the Moderate Resolution Imaging Spectroradiometer (on EOS) (MODIS), the Atmospheric Infrared Sounder (AIRS), and to simulated data. TES measures in the infrared spectral region (650–2260 cm^{-1}), where clouds have a ubiquitous impact on measured radiances and therefore on trace gas profile retrievals. The radiance contribution of clouds is parameterized in TES retrievals in terms of a set of frequency-dependent nonscattering effective optical depths and a cloud height. This unique approach jointly retrieves cloud parameters with surface temperature, emissivity, atmospheric temperature, and trace gases such as ozone from TES spectral radiances. We calculate the relationship between the true optical depth and the TES effective optical depth for a range of single-scatter albedo and phase functions to show how this varies with cloud type. We estimate the errors on retrieved cloud parameters using a simulated data set covering a wide range of cloud cases. For simulations with no noise on the radiances, cloud height errors are less than 30 hPa, and effective optical depth follows expected behavior for input optical depths of less than 3. When random noise is included on the radiances, and atmospheric variables are included in the retrieval, cloud height errors are approximately 200 hPa, and the estimated effective optical depth has sensitivity between optical depths of 0.3 and 10. The estimated errors from simulation are consistent with differences between TES and cloud top heights and optical depth from MODIS and AIRS.

Citation: Eldering, A., S. S. Kulawik, J. Worden, K. Bowman, and G. Osterman (2008), Implementation of cloud retrievals for TES atmospheric retrievals: 2. Characterization of cloud top pressure and effective optical depth retrievals, *J. Geophys. Res.*, *113*, D16S37, doi:10.1029/2007JD008858.

1. Introduction

[2] Clouds are present over a large fraction of the Earth at any given time, are located throughout the troposphere, and vary over orders of magnitude in their optical depth [*Liou*, 1992]. This presents a challenge for infrared remote sensing, as clouds have a significant impact on infrared radiances. Consequently, estimates of trace gas profiles derived using remotely sensed measurements must account for clouds.

[3] Many different approaches have been applied to identify the presence of clouds in remotely sensed measurements, characterize their properties, and account for their impact on retrievals of geophysical parameters. These include look-up tables of reflectance ratios and channel differences for cloud characterization used in Moderate Resolution Imaging Spectroradiometer (on EOS) (MODIS) data processing [*Ackerman et al.*, 1998; *King et al.*, 2003, *Platnick et al.*, 2003], cloud top pressure and effective cloud fraction retrieval followed by clearing to remove cloud impact on retrievals [*Smith*, 1968; *Chahine*, 1974; *Susskind et al.*, 2003, 2006], and minimization of observed and calculated radiance using a massive database of precomputed profiles [*Stubenrauch et al.*, 1999a, 1999b]. The method implemented for the Tropospheric Emission Spectrometer (TES) operation retrieval is a different scheme, where the cloud top pressure and effective optical depth retrievals are estimated simultaneously with trace gas profile retrievals [*Kulawik et al.*, 2006].

[4] In this paper, we will characterize the performance of the TES retrievals of cloud top pressure, effective cloud optical depth, and their error estimates through simulations. We then compare the operational cloud products with other operational remote sensing data sets of cloud top pressure and effective optical depth. Section 2 reviews the TES approach, discusses the simulated data set, and describes the Atmospheric Infrared Sounder (AIRS) and MODIS

[1] Jet Propulsion Laboratory, California Institute of Technology, Pasadena, California, USA.

0148-0227/08/2007JD008858$09.00

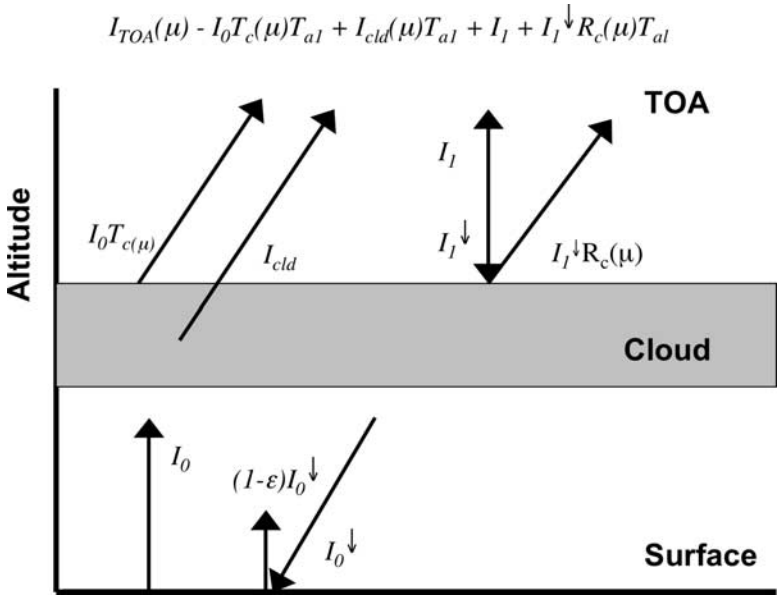

Figure 1. Schematic of IR radiative transfer in an atmosphere with a single-layer cloud (ray naming taken from *Wei et al.* [2004]).

cloud data that will be used in the comparisons. Section 3 focuses on the results of cloud retrieval for simulated data, and section 4 compares TES to other remote sensing data sets.

2. Data and Methods

2.1. TES

2.1.1. Forward Model Used for Clouds in TES Operational Retrievals

[5] As discussed by *Kulawik et al.* [2006], the forward model used by TES assumes nonscattering single-layer clouds, so we will first show how the TES retrieval parameter, effective optical depth, is related to the optical depth in the scattering case. The approach follows *Wei et al.* [2004] where the intensity coming from the top of the cloud (I_{cld}) in the general case is

$$I_{\mathrm{cld}} = [1 - R_c - T_c]B(t_c). \quad (1)$$

Here R_c and T_c are the reflection and transmission functions that come from complete multiple scattering radiative transfer function calculations. They are a function of ω (single-scatter albedo), g (Henley-Greenstein phase function parameter), and optical depth. The Planck radiance at temperature t is denoted by B, and t_c is the cloud temperature. Note that equation (1) and subsequent equations have an implicit frequency dependence. Placing this into the radiative transfer for a single cloud layer, as illustrated in Figure 1, the radiance at the top of the atmosphere is

$$I_{\mathrm{TOA}} = I_o T_c T_{a1} + [1 - R_c - T_c]B(t_c)T_{a1} + I_1 + I_1^{\downarrow} R_c T_{a1}. \quad (2)$$

In equation (2), I_{TOA} is the upwelling radiance at the top of the atmosphere (TOA), I_0 is the upwelling radiation at the cloud base, and T_{a1} is the transmission from TOA to the top of the cloud. The atmospheric radiation emitted above the cloud is I_1, while the downward radiation at the top of the cloud is $I_1^{\downarrow}$. All of these terms are illustrated in Figure 1. The TES forward model approximation assumes no scattering, a similar approach to the effective emissivity framework [*Platt and Stephens*, 1980; *Rathke and Fischer*, 2000, 2002]. This assumption results in the following equation for the radiance at the top of the atmosphere, where T'_c is the transmission function, assuming no scattering:

$$I_{\mathrm{TOA}} = I_o T'_c T_{a1} + \left[1 - T'_c\right]B(t_c)T_{a1} + I_1. \quad (3)$$

By combining equations (2) and (3), the relationship between the nonscattering (effective) and scattering cloud transmission is

$$T'_c = T_c + R_c\left[\frac{I^{\downarrow} - B(t_c)}{I_0 - B(t_c)}\right]. \quad (4)$$

[6] The parameter retrieved in the TES operational algorithm, effective optical depth, τ'_c, is simply related to the transmission function, $T'_c = \exp(-\tau'_c)$. *Kulawik et al.* [2006] showed that the nonscattering approximation, τ'_c, is valid for TES and that the errors incurred by using nonscattering clouds and Gaussian representation were comparable to the TES radiance errors. As will be discussed in section 3.1, *Toon et al.* [1989] have shown that T_c for forward scattering cases (positive g) is always greater than T_c for a nonscattering case ($\omega = 0$ and $g = 0$) of the same optical depth.

[7] The TES forward model does not attempt to connect the cloud effective optical depth back to scattering properties (ω, g), but rather to be formulated so that the cloud properties are retrieved well enough that the gas phase retrievals work well. Similarly, rather than determine the spectral dependence of the effective optical depth from cloud models, we simply retrieve this dependence with a

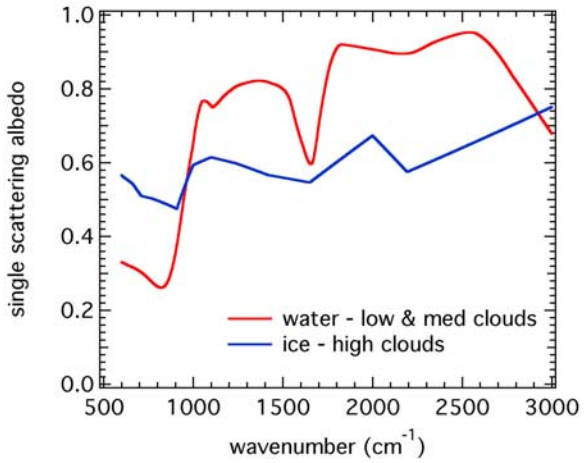

Figure 2. Single-scatter albedo as a function of wave number for the water and ice cloud models used in these simulations.

set of constraints described by *Kulawik et al.* [2006] that assume that the cloud effective optical depth is highly correlated over all frequencies. It should also be noted that calibration errors and spectroscopic errors with broad features cloud be aliased into the retrieved effective optical depth.

2.1.2. TES Operational Cloud Products

[8] The TES data product reports cloud effective optical depth and errors as functions of frequency and a cloud top pressure. There is a spectrally dependent effective cloud optical depth product as well as a spectrally averaged product. Cloud top pressure and error are also retrieved and reported in the level 2 data products. This paper is based on results from v002, and the simulations are performed with the same approach as in operational v002 retrievals.

2.2. Simulated Data

[9] Simulated radiances are calculated from profiles of ozone, temperature, water, as well as surface properties such as temperature and emissivity along with clouds. These simulated radiances are used to test the retrieval of cloud properties such as effective optical depth and cloud top height. These comparisons provide an indication of the accuracy of the TES retrievals as well as information about how scattering parameters influence the relationship between the input optical depth and the effective optical depth used in the TES forward model. For all of the simulations, the Code for High-Resolution Accelerated Radiative Transfer (CHARTS) model [*Moncet and Clough*, 1997] was used to generate the simulated radiances. CHARTS is a line-by-line radiative transfer model that uses the adding-doubling method to allow for scattering. These calculations were performed with an 87-layer atmosphere [*Beer et al.*, 1999] and assumed surface emissivity of 1.0.

[10] For the simulation studies, we consider three cases where there is no noise, and only the cloud parameters are retrieved (with all other parameters set to true). The purpose of these cases is to relate the retrieved effective optical depth to the actual effective optical depth for several different scattering cases, starting with the simplest limiting cases, and adding more realistic characteristics in steps. We also examine a case which has random noise added that follows the standard TES retrieval strategy (retrieving trace gases along with clouds, as described by *Kulawik et al.* [2006]. The cases are summarized as following: (1) no noise, nonscattering clouds (case NNNS); (2) no noise, isotropic clouds (case NNg0); (3) no noise, forward scattering clouds (case NNg76); (4) forward scattering clouds (like case NNg76) with noise following the standard TES retrieval strategy using a single tropical atmosphere (case WNGR); and (5) forward scattering clouds with noise following the standard TES retrieval strategy with a variable tropical atmosphere (case WNGR-atm).

[11] The three noiseless cases (NNNS, NNg0, and NNg76) are based on the same set of optical depths and cloud top pressures, and only the single-scatter albedo and phase function parameter are modified. For these cases, the clouds were placed at three different levels (301, 590, and 715 mbar), and only a single layer cloud is present. The clouds fill two model layers, where there are 24 layers per pressure decade (uniform in log pressure), so this is roughly 1.3 km, assuming a scale height of 7 km. The clouds at 301 mbar were modeled as ice clouds using the spectrally dependent properties of *Fu et al.* [1999], using an effective diameter of 50 μm. The midlevel (590 mbar) and low clouds (715 mbar) are modeled as water clouds with the spectrally dependent properties of *Hu and Stamnes* [1993], using an effective diameter of 5 μm. The single-scatter albedo of these clouds is illustrated in Figure 2. We see that the single-scatter albedo for the ice clouds has less spectral dependence than that for water clouds, and the water cloud single-scatter albedo changes rapidly between 800 and 1000 cm^{-1}. The phase function for the clouds is represented with Henley-Greenstein phase function and $g = 0.76$. The same atmosphere is used for all cases, a tropical atmosphere taken from a Model for Ozone and Related Chemical Tracer (MOZART)-3 run [*Brasseur et al.*, 1998].

[12] Cases WNGR and WNGR-atm represent complete simulations of TES retrievals, starting from a simulated radiance and using the standard TES initial guesses, constraints, and retrieval strategy, such as is described by *Kulawik et al.* [2006]. Unlike the above cases, NN. . ., these cases have noise added to the simulated radiance that is consistent with the TES noise equivalent spectral radiance. The retrieval strategy begins with the brightness temperature calculation and possible cloud initial guess refinement step when the brightness temperature difference is large, as discussed by *Kulawik et al.* [2006]. Following this step, cloud parameters (effective optical depth and cloud pressure) are retrieved in every step along with the atmospheric parameters of interest. Case WNGR-atm uses the same data set as used by *Kulawik et al.* [2006], which has tropical atmospheres taken from a MOZART-3 run. Case WNGR uses the same atmosphere for all cases (the 50th atmosphere from WNGR-atm) with variable clouds.

2.3. MODIS

[13] The MODIS instruments are 36-channel radiometers with spatial resolution ranging from 250 m to 1000 m, depending on the band. From these measurements, a wide set of atmospheric parameters are derived, including a cloud mask, cloud top pressure, cloud optical depth, and cloud effective radius [*King et al.*, 1992, 2003; *Platnick et al.*,

2003]. The cloud mask uses a complex cascade of tests to determining if a pixel is confidently clear, probably clear, probably cloudy, or cloudy. These tests include comparisons of brightness temperatures against thresholds, threshold tests of channel differences, and reflectance ratios. The cloud top pressure determination relies on the CO_2-slicing approach [*Menzel et al.*, 1983]. In cases where the CO_2-slicing approach fails, a method that relies on brightness temperature in the 11 μm atmospheric window (BT11) and an assumed emissivity of unity is employed [*Menzel et al.*, 2002].

[14] The cloud optical depth and particle size are retrieved using look-up tables of precalculated reflectance functions for channels ranging from the visible to 3.7 μm [*Platnick et al.*, 2003]. Along with the optical properties, the decision tree that was followed is archived with the data.

[15] There have been a number of reports comparing the cloud top heights retrieved by MODIS with ground-based lidar and radar cloud top heights [*Naud et al.*, 2002, 2004, 2005]. *Naud et al.* [2002, 2005] show that relative to the Galileo cloud radar at Chilboton and the Atmospheric Radiation Measurement program (ARM) (Department of Energy) southern Great Plains millimeter wavelength cloud radar, MODIS tends to overestimate slightly low cloud height and underestimate high clouds' cloud top heights. These statistics over a few dozen cases show MODIS cloud heights that range from 4 km less than the radar to 2 km greater. They conclude that MODIS CO_2-slicing cloud heights are underestimated for high thin clouds, and when clouds are optically thick, MODIS BT11 heights are above the radar cloud top heights. Comparisons with lidar-based cloud top heights [*Naud et al.*, 2005] shows that the difference between lidar and MODIS cloud top heights are $-1.2-1.5$ km for low clouds and between -1.4 and 2.7 km for high clouds.

2.4. AIRS

[16] EOS Aqua includes the AIRS/advanced microwave sounding unit (AMSU) instrument suite. The AIRS instrument is a grating spectrometer with 2378 channels in the spectral region from 650 cm^{-1} to 2675 cm^{-1} [*Aumann et al.*, 2003]. AIRS has a 13 km circular field of view (FOV) at nadir, and nine AIRS FOVs are captured in one AMSU-A footprint. This instrument suite was designed to provide radiosonde-quality temperature and water vapor profiles globally [*Tobin et al.*, 2006; *Divakarla et al.*, 2006]. These profiles are obtained with a two-part retrieval algorithm that relies on regression and physical retrievals described in detail by *Susskind et al.* [2003, 2006]. As part of that retrieval scheme, cloud fraction and cloud top pressure are retrieved. The clouds are treated as having up to two layers with an assumed spectral emissivity of 0.9 at all frequencies, and cloud fraction and cloud top temperature are retrieved for each of the AIRS field of views [*Susskind et al.*, 2003].

[17] *Kahn et al.* [2007] include a comparison of AIRS cloud top heights with measurements made at the ARM sites with cloud radar and lidar. These analysis show that the AIRS cloud top heights difference from the ARM site radar of -2.2 km to 1.6 km at Manus Island over 57 cases. Comparison to the lidar at Nauru shows AIRS-lidar differences of $-1.1-2.1$ km over 51 cases.

3. Characterization of Optical Depth and Cloud Top Pressure Retrieval From Simulations

3.1. Relationship Between Effective and Input Optical Depth

[18] In this section, we will explore the relationship between the cloud optical depth used in the CHARTS algorithm to create simulated radiances and the estimated effective optical depth from the TES retrieval algorithm, starting from the theoretical relationship between the effective transmission function and the true transmission function in equation (4). We transform equation (4) from describing the effective transmission function into effective optical depth, τ, using $t = \exp(-\tau)$, in order to compare it with the TES retrieval quantity.

[19] Discrete ordinates radiative transfer model (DISORT) was used to calculate the transmission function for the $g = 0$ and $g = 0.76$ cases. We verified our setup of DISORT by replicating results reported by *Hunt* [1973], *Toon et al.* [1989], and *Liou* [1992]. To introduce the relative magnitude of the reflectance and transmission functions, Figure 3 shows the transmission functions for four single-scattering albedos and two asymmetry factors, assuming a nadir viewing geometry, where the viewer is 180° from the emitting surface. We see that the isotropic scattering cases ($g = 0.0$) have transmission functions that are close to the nonscattering transmission, while the reflectance function ranges from 0.05 to 0.3, increasing with increasing single-scatter albedo. The transmission functions for the forward scattering model ($g = 0.76$) are larger than for the isotropic scatterer ($g = 0.0$), and the reflectance functions are about 1 order of magnitude smaller than the isotropic scattering case. This is a replication of the results of *Hunt* [1973] and *Toon et al.* [1989], and it is useful to consider the relative importance of terms in equation (4). For single-scatter albedos between 0.4 and 0.6 and $g = 0.76$, like the ice clouds of Figure 2, the reflectance function is between 0.01 and 0.02. In all cases, the transmission function for scattering particles is larger than the nonscattering transmission.

3.1.1. Calculating $T'c$ From Simulations

[20] In this section, we show the effective optical depth calculated with DISORT and CHARTS for representative cases. To simplify the analysis, we will focus on two frequency intervals, 850 cm^{-1}, where gas absorption is small, and 1075 cm^{-1}, where ozone absorption is important. Equation (4) can be fully evaluated from simulations, using T_c and R_c from DISORT and the upwelling and downwelling radiance at the upper and lower edge of the cloud from CHARTS. The average single-scatter albedos for the high, middle, and low cases at 850 cm^{-1} are 0.5, 0.35, and 0.35, respectively. At 1075 cm^{-1}, the single-scatter albedos of the modeled clouds are 0.6, 0.75, and 0.75, respectively. The data displayed in Figure 3 were interpolated to these single-scatter albedos for the calculation of $T'c$.

3.1.2. Isotropic Scattering Case

[21] The predicted and retrieved effective optical depths for the isotropic scattering case ($g = 0.0$) are shown in Figure 4. For the isotropic scattering, the effective optical depth is larger then the nonscattering optical depth for the middle and low clouds, and the reflectance term is more

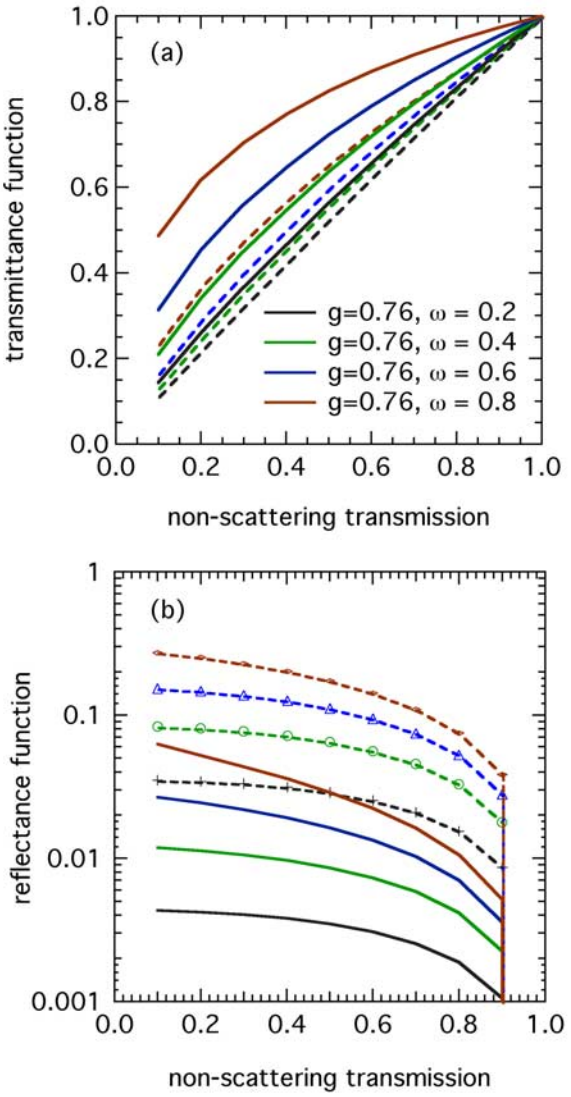

Figure 3. The transmission and reflectance functions as calculated with DISORT for a range of single-scatter albedos (indicated by color) and phase function parameters $g = 0.76$ (solid line) and $g = 0.0$ (dashed line).

important than the $g = 0.76$ case, as seen in Figure 3. The low clouds, represented by water clouds, have higher single-scatter albedo than the ice clouds, and this further increases the importance of the reflectance term.

3.1.3. Forward Scattering Case

[22] The analysis for $g = 0.76$ cases is focused on two frequencies, 850 and 1075 cm^{-1}. The input and effective optical depths are shown in Figure 5. In all cases, the effective optical depth is smaller than the input optical depth. This is consistent with the transmission function relationships shown in Figure 3 and can be explained by the fact that light is preferentially scattered in the forward direction, effectively reducing the cloud optical depth. The wavelength dependence is related to all terms in equation (4), including the single-scatter albedo, as well as the spectra dependence of the downwelling radiation that plays a role in the magnitude of the reflectance term.

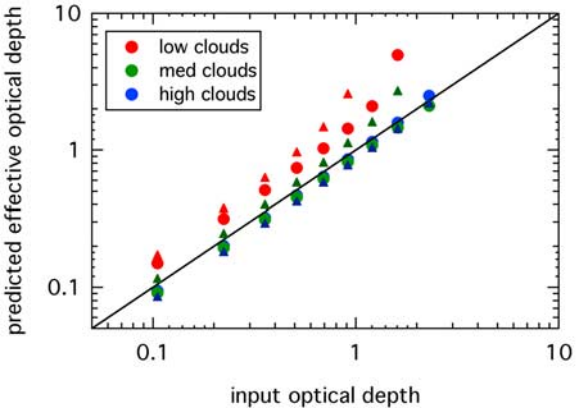

Figure 4. Predicted effective optical depth as a function of input optical depth for isotropic scattering cases ($g = 0.0$). These use reflectance and transmission functions representative of the ice and water clouds described in Figure 2. Circular symbols denote 850 cm^{-1}, and triangular symbols mark 1075 cm^{-1}.

3.2. Cloud Optical Depths Retrievals

[23] Retrieved effective optical depths are compared to the known true optical depth for all cases at a window frequency (975 cm^{-1}) with the retrieved effective optical depth plotted versus the true optical depth. Figure 6 shows the noise-free results. In Figure 6a, the nonscattering case (NNNS), the retrieved, and true optical depths follow the 1:1 curve until the cloud is opaque. For the TES cloud parameterization, which has a Gaussian shape versus pressure, an opaque cloud at one pressure is essentially equivalent to an optically thicker opaque cloud at a higher pressure. Both clouds could have the same large optical depth at the same pressure. In Figures 6b and 7b, we see that the retrieved optical depths are too high, but this is compensated for by placing the cloud lower in the atmosphere. This point is illustrated in Figure 8, where we have plotted

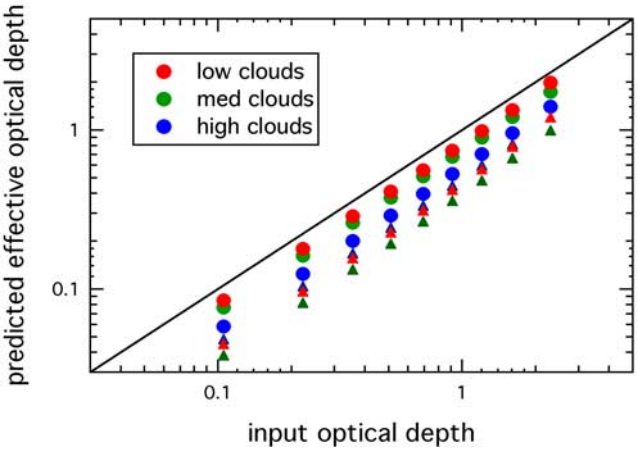

Figure 5. Predicted effective optical depth as a function of input optical depth for realistic scattering cases ($g = 0.76$). These use reflectance and transmission functions representative of the ice and water clouds described in Figure 2. Circular symbols denote 850 cm^{-1}, and triangular symbols mark 1075 cm^{-1}.

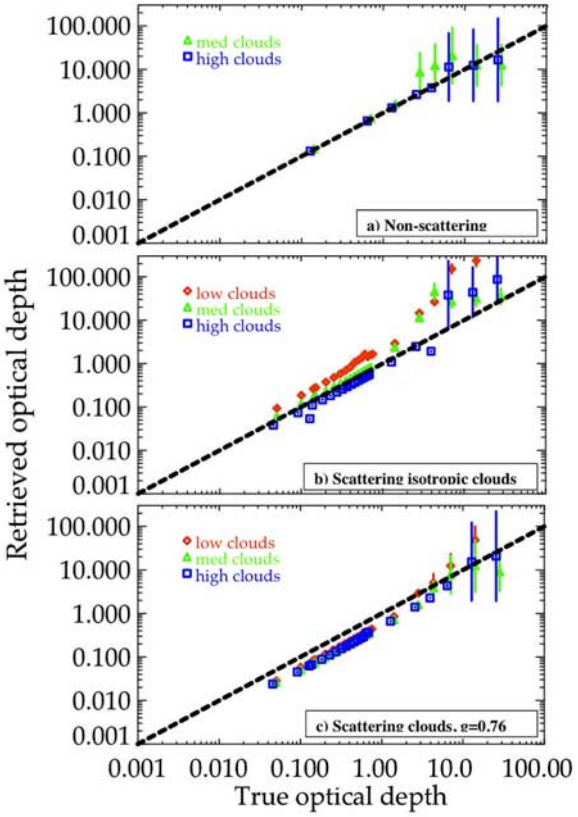

Figure 6. Retrieved effective optical depths plotted versus the input optical depths. (a) The nonscattering case (NNNS). The retrieved and true optical depths follow the 1:1 curve until the cloud is opaque. (b) The isotropic case (NNg0). (c) The $g = 0.76$ scattering case (NNg76).

the input and retrieved cloud effective optical depths as a function of pressure, as represented by the TES forward model. Although the total effective optical depth is quite different between the input and retrieved optical depths, 5.9 versus 20.2, respectively, both reach an optical depth of near 3 (which is 95% opaque) at 600 mbar because of the difference in cloud top heights. Thus they would appear similar in top of the atmosphere radiance. For the isotropic case (NNg0), shown in Figure 6b, the retrieved effective optical depths are higher than the true optical depths for low and medium clouds, and slightly lower than the true optical depth for the high clouds. The $g = 0.76$ scattering case (NNg76), shown in Figure 6c, shows the low clouds having consistently retrieved effective optical depths larger than the input optical depth, and higher clouds having consistently lower optical depths than the input optical depths. These results are consistent with the relationship between effective and true optical depth shown in equation (4) and illustrated in Figures 4 and 5.

[24] The retrievals that include TES noise and follow TES v002 processing, shown in Figure 7, are somewhat more interesting and relevant to results seen in TES operational data. Both Figures 7a (case WNGR) and 7b (case WNGR-atm) show that the TES-reported effective optical depths above 0.3 show a fairly monotonic sensitivity to the input optical depth. The effective optical depths below about

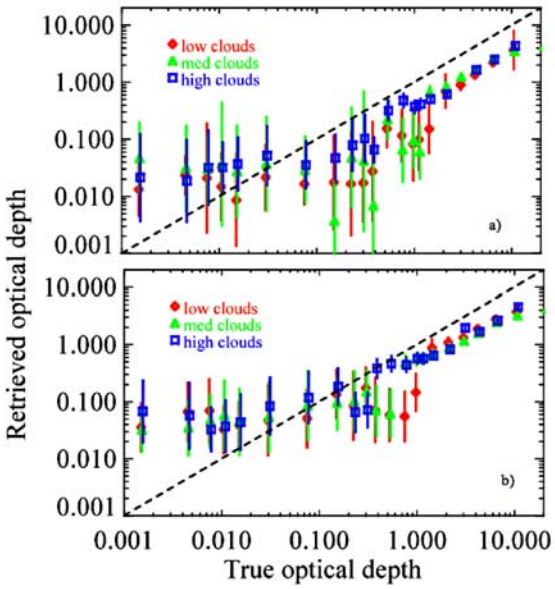

Figure 7. Retrieved effective optical depths plotted versus the true optical depths for the noise-added, full-retrieval cases with (a) the same cloud cases and true atmosphere as Figure 6 and (b) the same clouds in a variable tropical atmosphere.

0.3 do not show much sensitivity to the input optical depth. The high-optical depth cases surprisingly show more consistency than the noise-free results. The reason for the flattening at about approximately 0.04 optical depth is most likely from the retrieval strategy and the relationship between the surface temperature and atmospheric temperature used in these simulations. The a priori for clouds for low-optical depth cases are always set to 0.015 with TES v002 software. This leads to the elbow-shaped curve that flattens out at approximately 0.04 optical depth (surprisingly,

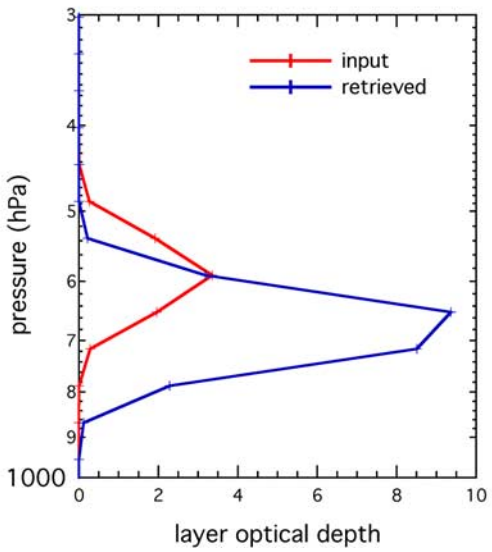

Figure 8. Profile of effective optical depth as input and retrieved with both optical depth profiles reaching 3 at 600 mbar.

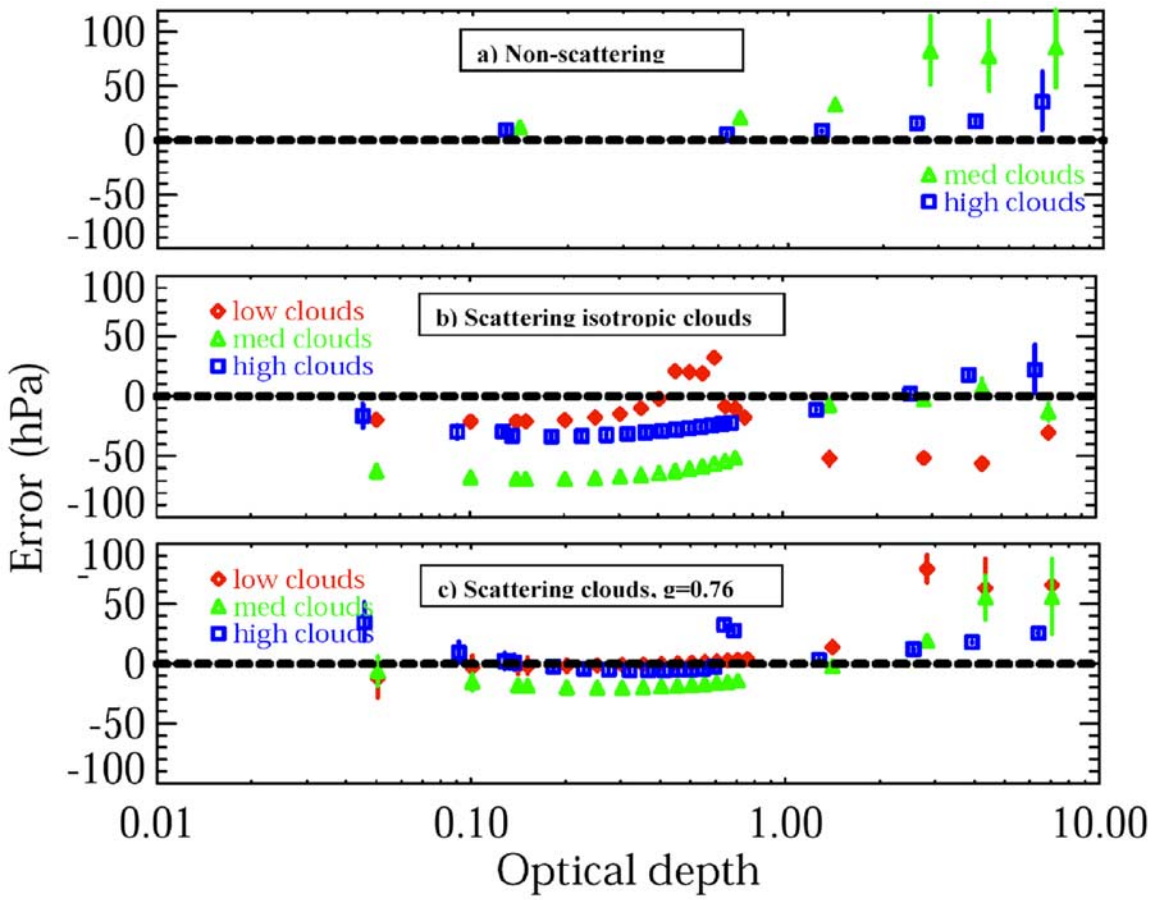

Figure 9. Error in the retrieved cloud top pressure (retrieved minus truth) as a function of cloud optical depth for (a) the nonscattering simulation cases (NNNS), (b) the isotropic scattering cases (NNg0), and (c) the scattering, $g = 0.76$ cases (NNg76). These cases have no noise added to the radiance, and all parameters start off at "true."

a larger value than 0.015). TES version v003 data sets the a priori cloud optical depth to much lower values, and this elbow is substantially improved for v003 data. Fifty percent of these cases were marked as "bad" by the master quality flag because of the emission layer flag (discussed in the Data Users Guide); however, all results are shown because the flagged cases were not significantly different. Note that retrieved optical depth from the actual, not simulated, TES products for v002 do not show this elbow, and whether this is due to actual sensitivity to low optical depths or to other factors needs to be tested with a more comprehensive data set including a wider range of atmospheric and surface conditions.

3.3. Cloud Top Pressure Retrievals

[25] In this section, we will show comparisons of the cloud top pressure that was retrieved and the value used as input to the simulation. It is important to note some differences in how the TES and CHARTS forward models process clouds. In the TES forward model, a cloud has a Gaussian shape in altitude with the cloud width approximately equal to one TES level (about 1 km) [*Kulawik et al.*, 2006]. In the CHARTS forward model, the cloud is turned "on" or "off" in a given layer. The true cloud top pressure for the simulations is set to the mean pressure of the cloud layer, whereas in the TES forward model, the retrieval pressure is the center pressure of the Gaussian distribution of the cloud, as was discussed in section 3.2 in reference to the optical depth retrieval. This may result in differences, especially when the optical depth is large because the cloud may be opaque several layers above the "center" of the cloud.

[26] Figure 9a shows the estimated and actual error (retrieved minus true) of retrieved cloud top pressure for the nonscattering simulation set. We see that the cloud top pressure for the high-altitude cloud is retrieved with actual errors of less than 10 hPa for optical depths less than 1. The estimated error is calculated assuming only measurement error and does not include the errors introduced by atmospheric profile error from temperature and water, and the errors for "real" retrievals are expected to be much larger. For the medium clouds, the actual cloud pressure error is about 10 hPa for thin clouds and then increases to about 80 hPa at optical depth 3 clouds. When looking at the retrieved optical depths, it is seen that the retrieval has placed a thicker cloud lower in the atmosphere. This will appear the same to the TES forward model when the cloud is opaque, as discussed in section 3.2.

[27] The errors of the retrieved cloud top pressure, seen in Figure 9b, are larger for the $g = 0.0$ case. The error in the

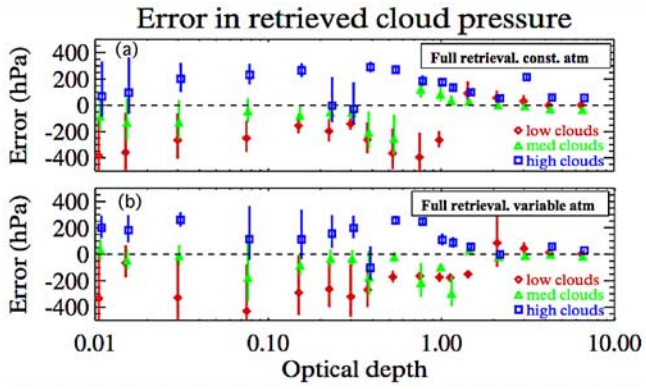

Figure 10. Error in the retrieved cloud top pressure (retrieved minus truth) as a function of cloud optical depth for the noise-added, full-retrieval cases with (a) the same cloud cases and true atmosphere as Figure 6 and (b) the same clouds in a variable tropical atmosphere.

retrieved cloud top pressure for the scattering case with g = 0.76 is shown in Figure 9c. Here we see that the actual cloud top retrieval error is less than 10 hPa for high and low clouds and on the order of 20 hPa for midaltitude clouds up to optical depths of 2, and then the errors become larger. The errors for the high clouds tend to be smallest for larger optical depth clouds. Overall, the estimated errors are small, and they are under-predicted for effective optical depths greater than 3.

[28] Figures 10a and 10b show the error of the retrieved cloud top pressure and the estimated error for TES-simulated retrievals of cloudy atmospheres where TES radiance noise has been used. The reported errors now include the propagation of uncertainties in the atmospheric temperature, surface temperature, and water vapor into errors in cloud properties and represent expected errors for retrievals using TES data. For the medium-height clouds, the reported and actual errors match fairly well, with most cases having the error bars crossing over or near to the zero line. High clouds are typically biased to a larger cloud top pressure, and low clouds are typically biased to a smaller cloud top pressure, even in the 0.4–1.5 optical depth range where the reported errors are quite small, but the actual errors are in the 200 hPa range. In most cases, the high clouds end up too low, and the low clouds end up too high. This indicates that the retrieved results tend to stay near the a priori value (which is always set to 500 hPa). For low optical depths, this is explained by the averaging kernel being less than 1. For the 0.4–1.5 cloud optical depth range, the retrieved cloud pressure has actual errors significantly larger than the reported errors, which indicates that the retrieval is converging to a local rather than global minimum. Corroborating this, the cloud pressure averaging kernel in this region indicates good sensitivities with values larger than 0.95.

[29] Analyses were performed to assess the impact of the cloud thickness assumed in the retrieval on the cloud top pressure. The assumption of one model layer used in the TES retrievals is close to the width used in the simulations, although the simulations used a block function, whereas TES uses a Gaussian-shaped cloud in log(pressure) [*Kulawik et al.*, 2006]. When the Gaussian half width was closer to one quarter of a TES layer, the retrieved cloud top pressure errors became near zero for all optical depths and clouds at all levels. If the retrieval model used clouds that were four model layers in width, the cloud top pressure retrievals for high clouds were barely changed, but for low clouds, the errors grew to more than 200 mbar for all optical depths. These analyses suggest that using a model that is close to or less than actual cloud width will not bias the cloud top pressure retrievals.

4. Results on Comparisons of TES, MODIS, and AIRS

4.1. Cloud Top Pressure

4.1.1. MODIS

[30] TES and MODIS data were chosen for five TES global surveys from August 2005 to March 2006. The MODIS data closest in space to TES were selected for comparison, and the data are always colocated within 0.5 km and approximately 15 min in time. Daytime and nighttime data were included in the analysis. We only use data that are identified as "confidently cloudy" by the MODIS cloud mask, and we use MYD06 cloud optical thickness and cloud top pressure products. The cloud parameters are not a primary product for TES but are required to make trace gas retrievals possible, and much of the retrieved cloud data are not recommended for scientific use. Thus data are selected for this comparison that has relatively small estimated errors. We have only selected TES data with a cloud top pressure error estimate of less than 100 mbar and an optical depth error estimate that is less than 2 times the reported optical depth. The data set contains 5791 footprints. Figure 11a illustrates the range of effective cloud optical depth and cloud top pressure from the TES operational retrievals that are compared to the MODIS retrieval products. The cloud top pressure and effective optical depth errors are small for middle to high clouds with optical depths greater than 1. Clouds with retrieved effective optical depths of less than 1 generally have large estimated errors in both optical depth and cloud top pressure. Figure 11b shows the distribution of cloud top pressures and effective cloud optical depths in one global survey of TES data, where all are data flagged as good (species retrieval quality = 1). There are many clouds reported with optical depth between 0.01 and 0.1 and from 0.5 to 10, and this distribution is representative of TES global survey data sets.

[31] Analysis of the aggregate (TES-MODIS) cloud top pressure differences shows that the mean difference is ~70 mbar, and 87% of the cases have cloud top pressure differences in the range of −200–200 mbar. Note that the Gaussian formulation of cloud effective optical thickness in the TES retrievals will place clouds at slightly higher pressure than a slab layer cloud representation. In Figure 12, histograms are shown for smaller groups of data selected by TES-retrieved optical depth and cloud top pressure. Figure 12b shows cases with retrieved effective optical depths greater than 3, and these show much narrower distributions of difference in cloud top pressure. The mean values range from 50 mbar to 100 mbar, but all have more than 70% of cases with differences between 0 and 120 mbar. For the cases where TES-retrieved effective optical depth is

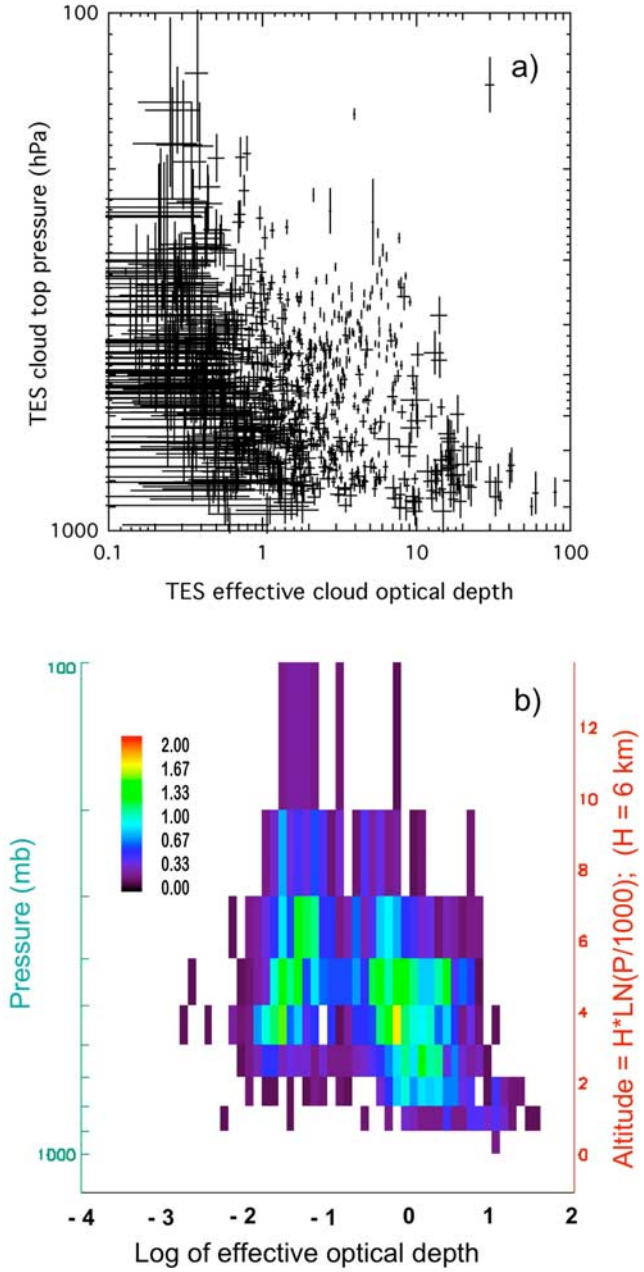

Figure 11. (a) TES-retrieved cloud top pressure and effective cloud optical depth for one global survey (3–4 March 2006) with estimated errors. (b) The frequency of occurrence (in percent) of cloud top pressure and cloud effective optical depths in one TES global survey.

less than 3 (Figure 12a), there are broad tails in the cloud top pressure differences. From the simulations with noise (see Figure 10), we see that cloud top pressure for high clouds is overestimated, while cloud top pressure for low clouds is underestimated. The biases reported between MODIS and ground-based lidars are in the same directions. An analysis of the differences of cloud top pressure between lidars and infrared measurements by *Holz et al.* [2006] shows that the infrared cloud top correlates with the unity optical depth level of the cloud lidar measurements. This is consistent with the biases of MODIS and lidars, and TES shows the same behavior. For effective optical depths less than 3, the difference between TES and MODIS is between −80 and 80 mbar for 76, 54, and 44% of cases for high, middle, and low clouds, respectively.

[32] The distribution of cloud top pressure differences is related to the initial guess and sensitivities of the two retrieval schemes. TES cloud top pressure initial guess and a priori value is 500 mbar in all cases, and in low-optical depth cases where there is little sensitivity, the cloud top pressure will tend toward this value. MODIS, on the other hand, uses a cloud top pressure first guess of 1000 mbar. Figure 13 shows the cloud top pressure differences (colors of dots) on TES cloud top pressure/effective optical depth coordinates (Figure 13a) and on MODIS cloud top pressure/effective optical depth coordinates (Figure 13b). These figures show that there are large differences for clouds that MODIS characterizes as near the surface, and

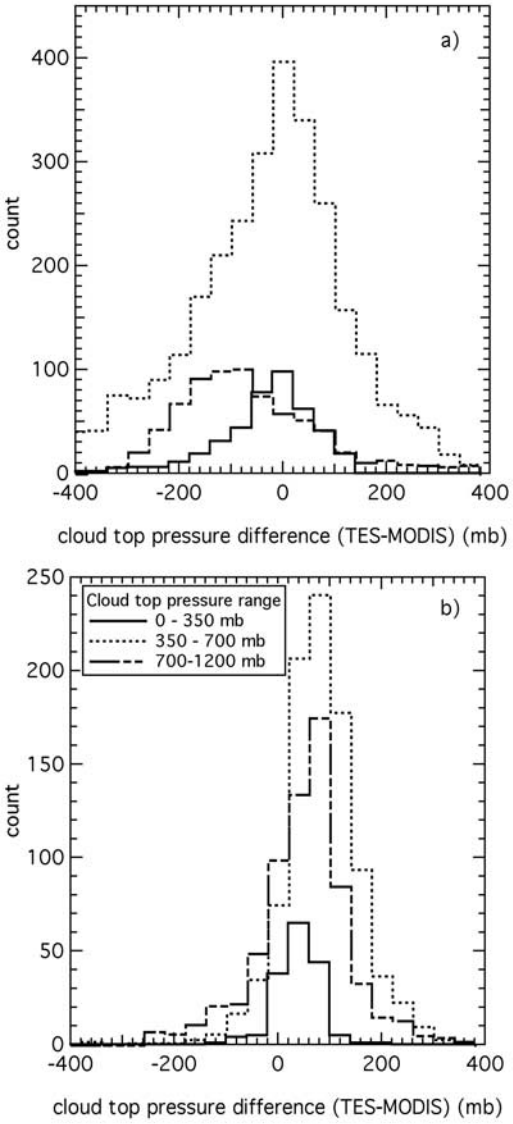

Figure 12. Histogram of differences in cloud top pressure (TES-MODIS) grouped by TES-retrieved cloud top pressure and optical depth, showing TES effective optical depths (a) less than 3 and (b) greater than 3.

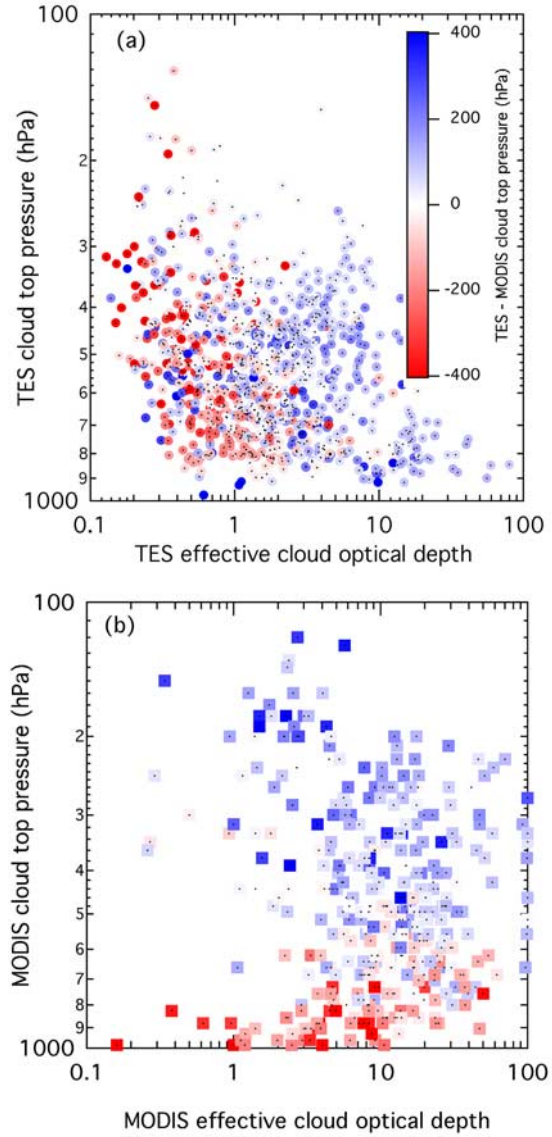

Figure 13. TES-MODIS cloud top pressure differences plotted in (a) TES-retrieved cloud top pressure and effective optical depth coordinates and (b) MODIS-retrieved cloud top pressure and effective optical depth coordinates. Dots are plotted for all cases, and colors are used to indicate the cloud top pressure difference.

these clouds are primarily characterized as low effective optical depths in the TES retrievals. Note that there are fewer cases in Figure 13b, as MODIS retrieves cloud top pressure for daytime and nighttime, but effective optical depth is only retrieved in daytime scenes.

4.1.2. AIRS

[33] Comparison of AIRS and TES cloud top pressures were also made. AIRS clouds retrievals allow for two cloud layers, whereas TES retrievals only account for one. Therefore we selected AIRS cases that indicated a single layer. This was defined as cases where the average AIRS cloud fraction on a 45 × 45 km footprint was less than 0.05 for one layer and greater than 0.2 for the other cloud layer. Approximately one third of AIRS- and TES-matched footprints met these criteria.

[34] We analyzed the TES-AIRS cloud top pressure differences for 16 global surveys taken between July 2005 and December 2005, containing 8567 cases. This histogram is sharply peaked between 0 and 100 mbar, indicating that TES places clouds lower than AIRS, and the histogram is more symmetric than the TES-MODIS histogram. The mean difference is 50 mbar, and 69% of the data are between −60 and 160 hPa in difference. Again, some cloud top pressure difference is expected because of the Gaussian representation of effective cloud optical depth in TES retrievals. Figure 14 shows histograms for data grouped by TES-retrieved optical depth and cloud top pressure, as in Figure 12. The characteristics are similar to MODIS, with a

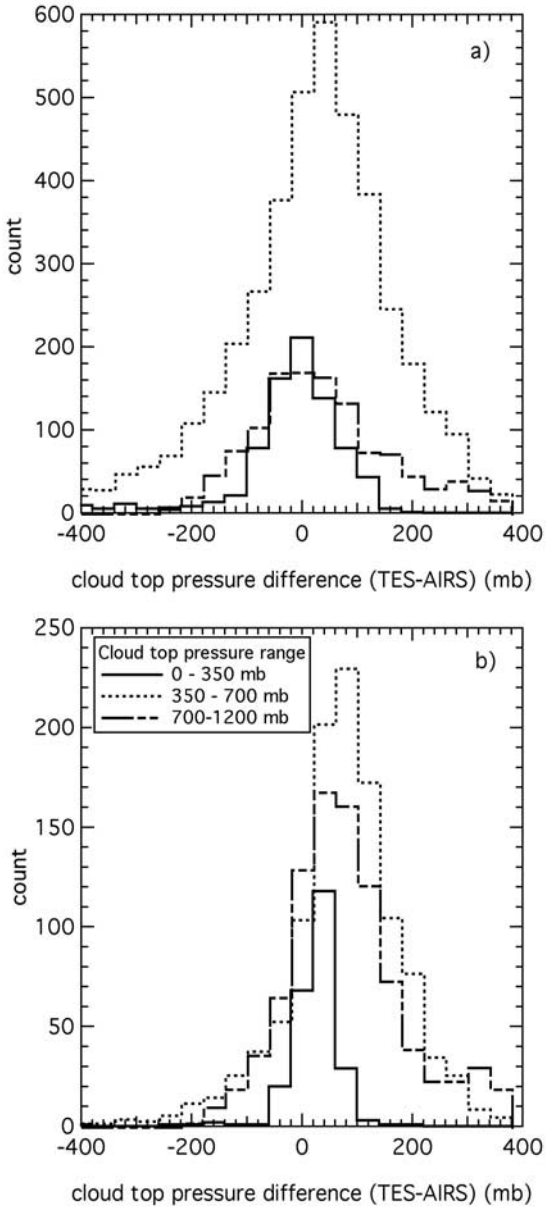

Figure 14. Histogram of differences in cloud top pressure (TES-AIRS) grouped by TES-retrieved cloud top pressure and optical depth, showing TES effective optical depths (a) less than 3 and (b) greater than 3.

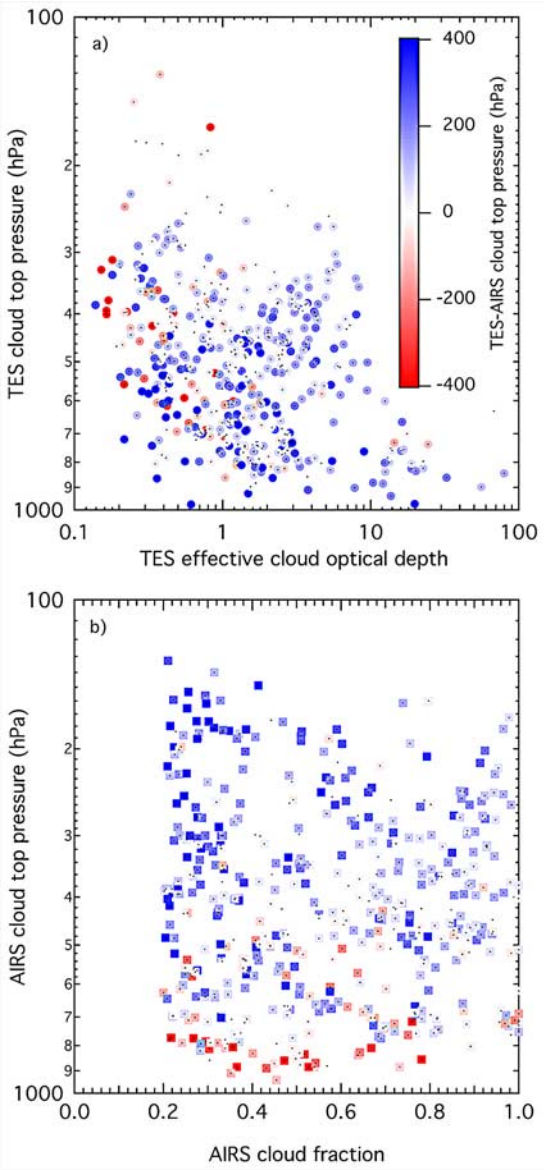

Figure 15. TES-AIRS cloud top pressure differences plotted in TES-retrieved cloud top pressure and (a) effective optical depth coordinates and (b) cloud fraction coordinates. Dots are plotted for all cases, and colors are used to indicate the cloud top pressure difference.

narrow distribution of differences for the higher, optically thicker clouds (Figure 14b) and broad tails in the distribution of differences for the low and middle clouds of thinner optical depth. The histograms of data for optical depths less than 3 (Figure 14a) are more symmetric than the TES-MODIS histograms, and the peak of the histogram has little dependence on the cloud top pressure. Although the retrieval approaches of TES and AIRS are quite different, they use a similar set of frequencies in the cloud retrievals for all conditions, which contributes to more similarity and symmetry of the cloud top pressure difference between TES and AIRS than TES and MODIS, as MODIS retrievals use channels that vary with cloud conditions.

[35] Plots of the cloud top pressure differences on the TES-retrieved cloud top pressure and effective optical depth and on the AIRS cloud top pressure and effective optical depth, in Figure 15, show that the largest cloud top pressure differences occur for clouds that TES characterizes as low effective optical depth, which AIRS places either near the surface or as high clouds with a low cloud fraction.

4.2. Optical Depth Comparisons

[36] Figure 16 shows a plot of the ratio of TES- and MODIS-retrieved effective optical depth for cloud top pressure, focused on cases with effective optical depth less than 3. Figure 16 shows that the MODIS-retrieved optical depth is almost always less than the TES-retrieved quantity. This is expected for visible compared to infrared measurements and depends on cloud type, where the infrared-to-visible optical depth ratio in the range from 1:1.8 to 1:4 [*Minnis et al.*, 1993]. The distributions of the histograms are rather narrow especially for the high clouds.

5. Discussion

[37] We have shown results for a set of simulated cases using CHARTS, a scattering radiative transfer code. Noise-free simulations show the relationship between the effective cloud optical depth and the scattering cloud optical depth and show that the retrieved effective cloud optical depths are well explained by simulations. Simulations including random noise retrieved with the standard TES retrieval scheme and assuming an emissivity of unity show a monotonic relationship between the true and retrieved optical depth above 0.3, similar to the noise-free results. Estimated effective optical depths below about 0.3, however, do not show much sensitivity to the true optical depth, a consequence of the retrieval strategy for v002, which is described by *Kulawik et al.* [2006]. The retrieved cloud top pressure tends to be systematically biased toward the a priori value of 500 hPa, so high clouds tend to be reported

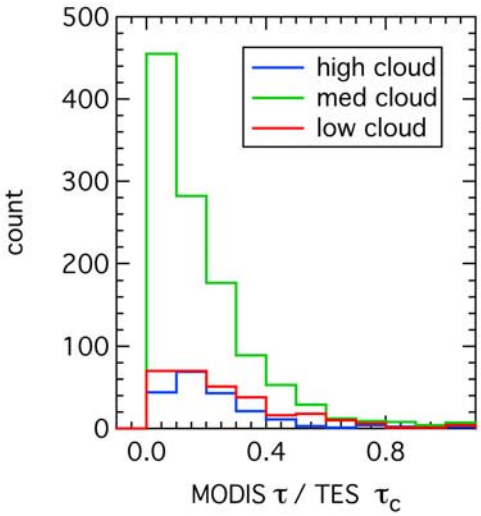

Figure 16. Histogram of the ratio of MODIS τ/TES τ_c grouped by TES-retrieved cloud top pressure for effective optical depths less than 3.

as too low and low clouds reported as too high. For thinner clouds, there is little sensitivity to the cloud top pressure, whereas for the thicker clouds, our analysis shows that we converge to a local minimum rather than a global minimum and are biased to the a priori as a result.

[38] When compared to other remote sensing data sets, we see that there is good agreement for cloud top pressure retrievals in comparisons of the mean values. There are a significant number of cases where there are differences of greater than 200 mbar. These are generally cases where TES retrieves a small optical depth across all altitudes, and MODIS or AIRS places the cloud near the surface or high.

[39] The results presented here are from TES v002 data. Processing of TES v003 data began in early 2007, and it will have different characteristics, as the cloud effective optical depth a priori is set with finer gradation and allows for lower values than in v002. In addition, v003 includes the CO_2 band (using frequencies 671–901 cm^{-1}) in retrievals, and this should result in more sensitivity in the cloud height retrievals. Along with assessing v003, future analysis will include a simulation study encompassing surface emissivity retrievals and a wider range of atmospheric conditions.

[40] **Acknowledgments.** This work was funded by the Jet Propulsion Laboratory, California Institute of Technology under contract to NASA.

References

Ackerman, S. A., K. I. Strabala, W. P. Menzel, R. A. Frey, C. C. Moeller, and L. E. Gumley (1998), Discriminating clear sky from clouds with MODIS, *J. Geophys. Res.*, *103*, 32,141–32,157, doi:10.1029/1998JD200032.

Aumann, H. H., et al. (2003), AIRS/AMSU/HSB on the Aqua mission: Design, science objectives, data products, and processing systems, *IEEE Trans. Geosci. Remote Sens.*, *41*, 253–264, doi:10.1109/TGRS.2002.808356.

Beer, R., et al. (1999), Tropospheric Emission Spectrometer (TES) level 2 algorithm theoretical basis document, *Doc. D-16474*, Jet Propul. Lab., Pasadena, Calif.

Brasseur, G. P., D. A. Hauglustaine, S. Walters, P. J. Rasch, J. F. Muller, C. Granier, and X. X. Tie (1998), MOZART, a global chemical transport model for ozone and related chemical tracers 1. Model description, *J. Geophys. Res.*, *103*, 28,265–28,289, doi:10.1029/98JD02397.

Chahine, M. T. (1974), Remote sounding of cloudy atmospheres. 1. Single cloud layer, *J. Atmos. Sci.*, *31*, 233–243, doi:10.1175/1520-0469(1974)031<0233:RSOCAI>2.0.CO;2.

Divakarla, M. G., C. D. Barnet, M. D. Goldberg, L. M. McMillin, E. Maddy, W. Wolf, L. Zhou, and X. Liu (2006), Validation of atmospheric infrared sounder temperature and water vapor retrievals with matched radiosonde measurements and forecasts, *J. Geophys. Res.*, *111*, D09S15, doi:10.1029/2005JD006116.

Fu, Q., W. B. Sun, and P. Yang (1999), Modeling of scattering and absorption by nonspherical cirrus ice particles at thermal infrared wavelengths, *J. Atmos. Sci.*, *56*, 2937–2947, doi:10.1175/1520-0469(1999)056<2937:MOSAAB>2.0.CO;2.

Holz, R. E., S. Ackerman, P. Antonelle, F. Nagle, R. O. Knuteson, M. McGill, D. L. Hlavka, and W. D. Hart (2006), An improvement to the high-spectral-resolution CO_2-slicing cloud-top altitude retrieval, *J. Atmos. Oceanic Tech.*, *23*, 653–670, doi:10.1175/JTECH1877.1.

Hu, Y. X., and K. Stamnes (1993), An accurate parameterization of the radiative properties of water clouds suitable for use in climate models, *J. Clim.*, *6*, 728–742, doi:10.1175/1520-0442(1993)006<0728:AAPOTR>2.0.CO;2.

Hunt, G. E. (1973), Radiative properties of terrestrial clouds at visible and infra-red thermal window wavelengths, *Q. J. R. Meteorol. Soc.*, *99*, 346–369.

Kahn, B. H., A. Eldering, A. J. Braverman, E. J. Fetzer, J. H. Jiang, E. Fishbein, and D. L. Wu (2007), Toward the characterization of upper tropospheric clouds using Atmospheric Infrared Sounder and Microwave Limb Sounder observations, *J. Geophys. Res.*, *112*, D05202, doi:10.1029/2006JD007336.

King, M. D., Y. J. Kaufman, W. P. Menzel, and D. Tanré (1992), Remote-sensing of cloud, aerosol, and water-vapor properties from the Moderate Resolution Imaging Spectroradiometer (MODIS), *IEEE Trans. Geosci. Remote Sens.*, *30*, 2–27, doi:10.1109/36.124212.

King, M. D., W. P. Menzel, Y. J. Kaufman, D. Tanré, B. C. Gao, S. Platnick, S. A. Ackerman, L. A. Remer, R. Pincus, and P. A. Hubanks (2003), Cloud and aerosol properties, precipitable water, and profiles of temperature and water vapor from MODIS, *IEEE Trans. Geosci. Remote Sens.*, *41*, 442–458, doi:10.1109/TGRS.2002.808226.

Kulawik, S. S., J. Worden, A. Eldering, K. Bowman, M. Gunson, G. B. Osterman, L. Zhang, S. Clough, M. W. Shephard, and R. Beer (2006), Implementation of cloud retrievals for Tropospheric Emission Spectrometer (TES) atmospheric retrievals: part 1. Description and characterization of errors on trace gas retrievals, *J. Geophys. Res.*, *111*, D24204, doi:10.1029/2005JD006733.

Liou, K. N. (1992), *Radiation and Cloud Processes in the Atmosphere: Theory, Observations, and Modeling*, Oxford Univ. Press, New York.

Menzel, W. P., W. L. Smith, and T. R. Stewart (1983), Improved cloud motion wind vector and altitude assignment using VAS, *J. Clim. Appl. Meteorol.*, *22*, 377–384, doi:10.1175/1520-0450(1983)022<0377:ICMWVA>2.0.CO;2.

Menzel, W. P., B. A. Baum, K. I. Strabala, and R. A. Frey (2002), Cloud top properties and cloud phase, version 6, *NASA Algorithm Theor. Basis Doc.*, *ATBD-MOD-04*.

Minnis, P., K.-N. Liou, and Y. Takano (1993), Inference of cirrus cloud properties using satellite-observed visible and infrared radiances. part I: Parameterization of radiance fields, *J. Atmos. Sci.*, *50*, 1279–1304, doi:10.1175/1520-0469(1993)050<1279:IOCCPU>2.0.CO;2.

Moncet, J. L., and S. A. Clough (1997), Accelerated monochromatic radiative transfer for scattering atmospheres: Application of a new model to spectral radiance observations, *J. Geophys. Res.*, *102*, 21,853–21,866, doi:10.1029/97JD01551.

Naud, C., J.-P. Muller, and E. E. Clothiaux (2002), Comparison of cloud top heights derived from MISR stereo and MODIS CO_2-slicing, *Geophys. Res. Lett.*, *29*(16), 1795, doi:10.1029/2002GL015460.

Naud, C., J.-P. Muller, M. Haeffelin, Y. Morille, and A. Delaval (2004), Assessment of MISR and MODIS cloud top heights through inter-comparison with a back-scattering lidar at SIRTA, *Geophys. Res. Lett.*, *31*, L04114, doi:10.1029/2003GL018976.

Naud, C. M., J.-P. Muller, E. E. Clothiaux, B. A. Baum, and W. P. Menzel (2005), Intercomparison of multiple years of MODIS, MISR and radar cloud-top heights, *Ann. Geophys.*, *23*, 2415–2424.

Platnick, S., M. D. King, S. A. Ackerman, W. P. Menzel, B. A. Baum, J. C. Riédi, and R. A. Frey (2003), The MODIS cloud products: Algorithms and examples from Terra, *IEEE Trans. Geosci. Remote Sens.*, *41*, 459–473, doi:10.1109/TGRS.2002.808301.

Platt, C. M. R., and G. L. Stephens (1980), The interpretation of remotely sensed high cloud emittances, *J. Atmos. Sci.*, *37*, 2314–2322, doi:10.1175/1520-0469(1980)037<2314:TIORSH>2.0.CO;2.

Rathke, C., and J. Fischer (2000), Retrieval of cloud microphysical properties from thermal infrared observations by a fast iterative radiance fitting method, *J. Atmos. Oceanic Tech.*, *17*, 1509–1524, doi:10.1175/1520-0426(2000)017<1509:ROCMPF>2.0.CO;2.

Rathke, C., and J. Fischer (2002), Efficient parameterization of the infrared effective beam emissivity of semitransparent atmospheric layers, *J. Geophys. Res.*, *107*(D4), 4035, doi:10.1029/2001JD000596.

Smith, W. L. (1968), An improved method for calculating tropospheric temperature and moisture from satellite radiometer measurements, *Mon. Weather Rev.*, *96*, 387–396, doi:10.1175/1520-0493(1968)096<0387:AIMFCT>2.0.CO;2.

Stubenrauch, C. J., W. B. Rossow, F. Chéruy, A. Chédin, and N. A. Scott (1999a), Clouds as seen by satellite sounders (3I) and imagers (ISCCP). part I: Evaluation of cloud parameters, *J. Clim.*, *12*, 2189–2213, doi:10.1175/1520-0442(1999)012<2189:CASBSS>2.0.CO;2.

Stubenrauch, C. J., A. Chédin, R. Armante, and N. A. Scott (1999b), Clouds as seen by satellite sounders (3I) and imagers (ISCCP). part II: A new approach for cloud parameter determination in the 3I algorithm, *J. Clim.*, *12*, 2214–2223, doi:10.1175/1520-0442(1999)012<2214:CASBSS>2.0.CO;2.

Susskind, J., C. D. Barnett, and J. M. Blaisdell (2003), Retrieval of atmospheric and surface parameters from AIRS/AMSU/HSB data in the presence of clouds, *IEEE Trans. Geosci. Remote Sens.*, *41*, 390–409, doi:10.1109/TGRS.2002.808236.

Susskind, J., J. Blaisdell, L. Iredell, F. Keita, L. Kouvaris, G. Molnar, R. Atlas, and M. Chahine (2006), Accuracy of geophysical parameters derived from atmospheric infrared sounder/advanced microwave sounding unit as a function of fractional cloud cover, *J. Geophys. Res.*, *111*, D09S17, doi:10.1029/2005JD006272.

Tobin, D. C., H. E. Revercomb, R. O. Knuteson, B. M. Lesht, L. L. Strow, S. E. Hannon, W. F. Feltz, L. A. Moy, E. J. Fetzer, and T. S. Cress (2006),

Atmospheric radiation measurement site atmospheric state best estimates for atmospheric infrared sounder temperature and water vapor retrieval validation, *J. Geophys. Res.*, *111*, D09S14, doi:10.1029/2005JD006103.

Toon, O. B., C. P. McKay, and T. P. Ackerman (1989), Rapid calculation of radiative heating rates and photodissociation rates in inhomogeneous multiple scattering atmosphere, *J. Geophys. Res.*, *94*, 16,287–16,301, doi:10.1029/JD094iD13p16287.

Wei, H., P. Yang, J. Li, B. A. Baum, H.-L. Huang, S. Platnick, Y. Hu, and L. Strow (2004), Retrieval of semitransparent ice cloud optical thickness from Atmospheric Infrared Sounder (AIRS) measurements, *IEEE Trans. Geosci. Remote Sens.*, *42*, 2254–2267, doi:10.1109/TGRS.2004.833780.

K. Bowman, A. Eldering, S. S. Kulawik, G. Osterman, and J. Worden, Jet Propulsion Laboratory, California Institute of Technology, 4800 Oak Grove Drive, Pasadena, CA 91109, USA. (annmarie.eldering@jpl.nasa.gov)